

Mesozooplankton and particulate matter responses to a deep-water frontal system in the southern California Current System

MARK D. OHMAN^{1*}, JESSE R. POWELL¹, MARC PICHERAL² AND DAVID W. JENSEN¹

¹CALIFORNIA CURRENT ECOSYSTEM LTER SITE, SCRIPPS INSTITUTION OF OCEANOGRAPHY, LA JOLLA, CA 92093-0218, USA AND ²UNIVERSITÉ PIERRE ET MARIE-CURIE PARIS 6 AND CNRS, LABORATOIRE D'Océanographie de Villefranche, 06230 VILLEFRANCHE-SUR-MER, FRANCE

*CORRESPONDING AUTHOR: mohman@ucsd.edu

Received November 3, 2011; accepted in principle March 15, 2012; accepted for publication March 20, 2012

Corresponding editor: Roger Harris

We analyzed the abundance of mesozooplankton and suspended particulate matter across the deep-water “A-Front” in the southern sector of the California Current System. We characterized the A-Front with two novel devices, a free-fall Moving Vessel Profiler (MVP) and an Underwater Vision Profiler 5 (UVP5), together with quantitative bongo samples analyzed by ZooScan. The MVP permitted real-time visualization of vertical density structure, chlorophyll *a* fluorescence and particle size structure (from a laser optical particle counter) across the front to a depth of 200 m with the research vessel moving at 6 m s⁻¹. The UVP5 quantified *in situ* vertical distributions from digital images of planktonic organisms and particles in profiles to 300 m. Both the MVP and UVP5 indicated that organic aggregates increased several-fold at the A-Front. The A-Front was a region of elevated abundance of mainly particle-grazing mesozooplankton, including calanoid copepods, *Oithona* spp., appendicularians and euphausiids, as well as a site of elevated ratio of nauplii copepod⁻¹. In contrast, poecilostomatoid copepods, ostracods, chaetognaths and radiolaria, most of which are more carnivorous or omnivorous, were all elevated in abundance to the south of the front. We provide evidence that submesoscale fronts can be regions of locally elevated plankton abundance and production, as well sites of faunal transitions.

KEYWORDS: fronts; copepods; mesozooplankton; secondary production; size spectra

INTRODUCTION

Plankton patchiness is ubiquitous in the ocean and present across a broad range of spatial scales (Haury *et al.*, 1978). For many years, “patchiness” in the California Current System (CCS) was analyzed essentially as a statistical phenomenon of increased variance of abundance. Focused studies subsequently revealed, in

many cases, a direct association between physically induced discontinuities in the water column and the distributions of planktonic organisms. Such phenomena range in scale from microscale thin layers in the vertical plane (Owen, 1991; Cowles *et al.*, 1998; Prairie *et al.*, 2010), submesoscale and mesoscale fronts (Mackas *et al.*, 1991; Smith and Lane, 1991) and eddies (Haury, 1984),

bathymetric features such as seamounts (Genin *et al.*, 1994) or changes in continental shelf topography (Barth *et al.*, 2005), to the consequences of large-scale ocean circulation and water mass relationships on the distributions of organisms (Brinton *et al.*, 1999). Davis *et al.* (Davis *et al.*, 2008) used *Spray* ocean gliders to resolve frontal features in the southern CCS, revealing a strong association between horizontal density features, phytoplankton chlorophyll *a* (Chl *a*) fluorescence and mesozooplankton acoustic backscatter. Belkin *et al.* (Belkin *et al.*, 2009) summarized the occurrence of quasi-stationary fronts in different ocean regions based on satellite thermal imagery and suggested that frontal features in the CCS become more organized and anisotropic in winter in comparison with summer.

In the present study, we examined the effects of a major deep-water oceanic frontal system on the distributions of mesozooplankton and suspended particulate matter. This front, which we designate the A-Front, was clearly visible in satellite sea surface temperature and ocean color imagery (Kahru *et al.*, 2012; Landry, Ohman *et al.*, 2012). It differed from fronts studied elsewhere in the CCS, in that it was not directly associated with a recent upwelling event (Peterson *et al.*, 1979) or with coastally derived filaments extending offshore (e.g. Mackas *et al.*, 1991; Smith and Lane, 1991). Nor was it associated with terrestrially derived freshwater inflow, tidally induced mixing and stratification (cf. Pingree and Griffiths, 1978; Hunt *et al.*, 1998), or with irregular topographic features such as the continental shelf break or seamounts. Rather, this was a feature offshore of the Southern California Bight in a region ~ 3800 m deep that lacked major seafloor discontinuities. Although fronts have been analyzed previously in the region (e.g. Haury *et al.*, 1993; Chereskin and Niler, 1994; Venrick, 2000), the A-Front gradient zone appears to have had markedly different characteristics. Here, we test the null hypothesis of no difference in mesozooplankton and particulate matter abundance and composition across a deep-water physical gradient region.

METHOD

The A-Front was initially identified from satellite imagery (Fig. 1, Kahru *et al.*, 2012; Landry, Ohman *et al.*, 2012) accessed at sea, then a preliminary site survey aboard the R/V *Melville* was conducted to localize the position of the front and guide more detailed sampling. The site survey (Fig. 2) was conducted with a free-fall Moving Vessel Profiler (MVP, ODIM Brooke Ocean; Herman *et al.*, 1998) deployed in the upper 200 m, and with a shipboard continuous underway

Advanced Laser Fluorometer (ALF) system (Chekalyuk *et al.*, 2012) sampling an uncontaminated seawater intake at ~ 4 m depth.

The MVP 200 permits vertical profiles to be made to a depth of 200 m with the ship moving continuously at speeds of 6 m s^{-1} (~ 12 knots). The free-fall MVP “fish” contains a laser optical particle counter (LOPC, Herman *et al.*, 2004), a Wetlabs FLRT Chl *a* fluorometer and an Applied Microsystems Micro CTD. The fish is suspended from a synthetic Vectran conducting cable, with all data displayed shipboard in real time. Initial launch and recovery of the MVP take a few minutes and entail temporarily slowing the vessel to $1\text{--}2 \text{ m s}^{-1}$, after which the ship can immediately be brought to full speed. The MVP is regulated by a computer-controlled winch system and operated remotely from within the shipboard laboratory. Upon a computer command, a brake is released, the winch freewheels and the fish falls freely through the water column under gravity at $3.5\text{--}4 \text{ m s}^{-1}$, with sampling unaffected by ship motion or sea state. At the desired hydrostatic pressure, the winch brake is automatically applied, then the MVP winch retrieves the fish through a controlled ascent, docking 2–4 m below the sea surface. A bottom avoidance algorithm is incorporated. The MVP can be set to cycle continuously, in which case vertical profiles are made at $\sim 2.5\text{--}3.5$ km horizontal intervals with the ship moving forward at $5\text{--}6 \text{ m s}^{-1}$. The MVP profiles on descent and ascent, although we used only the descent data because descents occur at a nearly constant speed and equal sampling effort is therefore allocated to each depth stratum. LOPC data are recorded at 2 Hz, providing ~ 2 -m vertical resolution, while the CTD and fluorometer are sampled at 25 Hz, providing ca. 0.08-m vertical resolution on descent. We subsequently binned the LOPC data into 3 m depth bins and the CTD and Chl *a* fluorescence data into 1-m bins. Temperature data were corrected for the sensor time lag prior to the calculation of salinity and density. The LOPC was calibrated with microspheres of glass (0.24 μm , 1.31 μm diameter) or nylon (7.1 μm diameter) before and after the cruise (BOT, 2005). The fluorometer was checked for dark current and full-scale response before field deployments and, in the laboratory, measured against an extract of pure Chl *a* (cf. Davis *et al.*, 2008) as well as a phytoplankton assemblage collected from the Scripps pier.

The site survey entailed five crossings of the A-Front: three initial crossings were conducted with the vessel moving at 5.5 m s^{-1} and MVP profiling at ~ 3.7 km intervals, extending well to the north and south of the front (Fig. 2). These were followed by two slower crossings at 2.9 m s^{-1} , which permitted 1.1 km

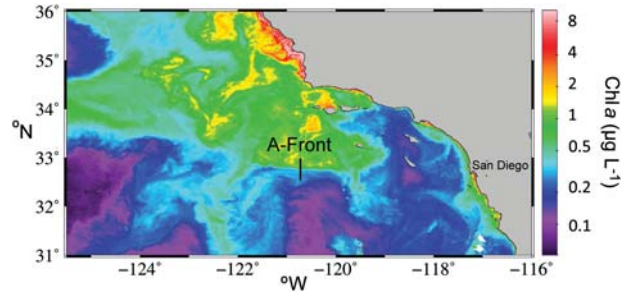


Fig. 1. Satellite image of Chl *a* in the southern sector of the CCS. Vertical black line indicates the location of the A-Front study. Chl *a* is merged for 22–25 October 2008 from MERIS, MODIS-Aqua, MODIS-Terra and SeaWiFS data; image courtesy of M. Kahru, SIO.

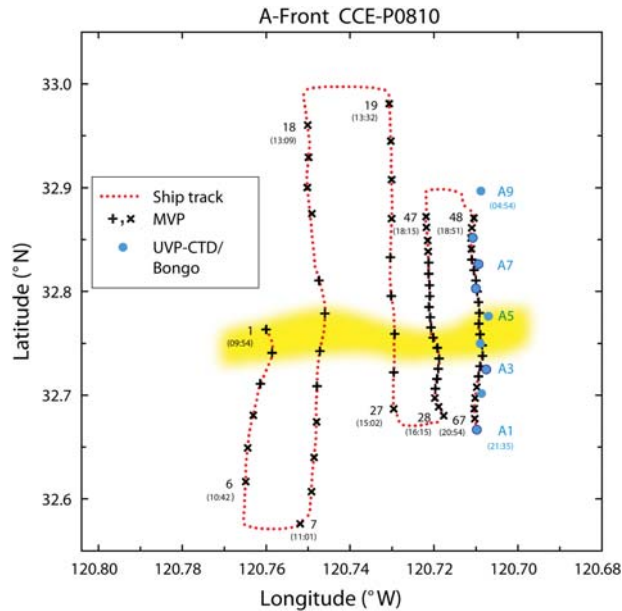


Fig. 2. Survey and sampling track across A-Front, 24–25 October 2008. Central yellow band indicates the core frontal area. Dotted line is the ship track and (+, ×) indicate MVP cast locations and cast numbers (1–67) with local time shown in black, where (×) identifies MVP casts clearly to the south or north of the front and beyond the transitional region. Locations of CTD–UVP5–Rosette and bongo samples shown as blue circles labeled A1–A9, with start times for the first and last stations.

horizontal resolution of the frontal gradients. After completion of the initial continuous site survey (09:54–20:54 local time, 24 October 2008), direct *in situ* sampling was carried out with a rapid series of CTD–Underwater Vision Profiler 5 (UVP5)–rosette and vertical bongo deployments completed entirely during nighttime hours (21:35–04:54 local time, 24–25 October 2008), at stations designated A1 through A9 (Fig. 2). For each CTD–UVP5–rosette/bongo station, the ship was stopped, the rosette bearing the UVP5 lowered to 300 m depth and recovered, then a vertically retrieved bongo net (0.71-cm diameter, 202- μm mesh; cf. Ohman and Wilkinson, 1989) deployed to a depth of 100 m and recovered at 30 m min^{-1} . Wire angles were maintained close to vertical and calibrated flow meter readings indicated that $\sim 40 \text{ m}^3$ were filtered per

sample. One plankton sample was preserved in 1.8% formaldehyde buffered with saturated sodium borate and the other frozen in liquid nitrogen for grazing determinations, but due to failure of a Dewar, the latter samples were lost. For the purpose of contrasting vertical profiles in the front with those on either side of it, a series of 11 MVP profiles in the “core” frontal region was identified by examining vertical profiles of *in vivo* Chl *a* fluorescence. Profiles in the core A-Front were contrasted with clusters of profiles well outside the influence of the front to the north ($n = 16$) and south ($n = 15$; see Fig. 2).

Ashore, the vertical bongo samples were analyzed by ZooScan digital scanning and image analysis (Gorsky et al., 2010). Samples were gently separated into two size fractions (0.2–1 mm, >1 mm) by sieving

through a plankton mesh, then two aliquots of each fraction were scanned at 2400 dpi resolution. Segmented vignettes (regions of interest) were initially classified by a machine algorithm using the Random Forest classification and regression tree method (Gorsky *et al.*, 2010), then 100% of the images were examined manually to correct mis-classifications. Abundances are expressed as number m^{-3} averaged over the upper 100 m, after correction for volumes filtered at sea and aliquot fractions.

The UVP5 is a digital camera system with columnar LED illumination at 625 nm that images 1 L of water with 100 μs flash pulses, recording images at 6 Hz while the instrument profiles vertically (Picheral *et al.*, 2010). In the shipboard configuration, the UVP5 measures objects larger than 100 μm and retains images of objects larger than 500 μm . The UVP5 was positioned at the lowest location on the CTD-rosette so that it sampled minimally disturbed water upon descent, profiling at a rate of 30 m min^{-1} to 100 m and 60 m min^{-1} in deeper depths. The summed abundance of organisms within a specified size window was displayed shipboard in real time during descent. Upon recovery, the full suite of acquired images was downloaded from the UVP. After image segmentation, vignettes were classified using the Random Forest algorithm. Machine classifications were subsequently verified manually.

The LOPC on the MVP employs a 35-element photodiode array to record attenuation of a 670-nm laser diode across a 70-mm wide sampling tunnel (Herman *et al.*, 2004). Light attenuation is proportional to particle size, which is expressed as equivalent spherical diameter (ESD). Single element particles (SEP's) intersect one (or at most two) elements 1 mm on a side, while multi-element particles (MEP's) cross more than two elements and are ≥ 1.5 mm in linear dimensions, although they can be < 1 mm in ESD. The LOPC is not an image-forming device, but for larger MEP's, the coarsely (1-mm pixel size) outlined silhouette of the object, together with the opacity of each pixel, can sometimes be interpreted in relation to known organism types. The opacity (scaled from 0 to 1, where 1 is completely opaque) of MEP's is the average proportion of light occluded across all affected photodiode elements except the end pixels of the object. The first and last pixels are excluded from this calculation because the particle often does not entirely cover these elements. Checkley *et al.* (Checkley *et al.*, 2008) suggested that objects with opacity > 0.6 and 1.1–1.7 mm ESD correspond to larger copepods in this part of the CCS, while lower opacity particles in this region tend to be dominated by marine snow. Gaardsted *et al.* (Gaardsted

et al., 2010) found lower values of opacity for *Calanus finmarchicus* in the Norwegian Sea.

The volume of water sampled was determined by multiplying the cross-sectional area of the LOPC sampling tunnel by its velocity, estimated by changes in pressure over known time intervals. We tabulated the number of MEP particle detections in each of the 35 LOPC diode element over many MVP casts, and found that the first three elements rarely registered any particles ($< 0.01\%$ of all detections). Thus, the volume of water sampled was somewhat less than that flowing through the tunnel. To compensate, the water volume sampled was calculated as 32/35 of the volume flowing through the tunnel. Our ratios of Total counts:MEP counts ranged from 28 to 43, exceeding the threshold of 20 below which Schultes and Lopes (Schultes and Lopes, 2009) reported as saturating the LOPC in turbid areas. Our proportion of incoherent MEP's (as defined by Schultes and Lopes 2009) averaged 0.5% and therefore did not bias the size distributions reported here.

Normalized particle volume spectra (nVd, Jackson *et al.*, 1997; Checkley *et al.*, 2008) were calculated from a combination of SEP and MEP particles. Particles were placed in logarithmic size bins, with the ratio of the largest to smallest particle size in each bin 1.1447. The particle number spectrum (n_{ij}) was estimated for particles sampled in the downcast (from ~ 7 to 200 m depth) in 3 m depth bins. For each size (i) and depth (j) bin, the number of particles was divided by the volume of water sampled and by the width of the size bin (Δd_i). The normalized volume spectrum (nVd) was then calculated by multiplying the n_{ij} by the volume of a particle (V) with a median ESD for that bin and by the median size (d) of the bin. The last operation normalizes the volume spectra so that when plotted on a logarithmic size scale, the area under the curve is proportional to the integrated particle volume. Size spectra were summed across all depths in a vertical profile for comparison of the front with waters to the north and south.

RESULTS

The A-Front was a region of relatively sharp horizontal gradients oriented approximately north–south, with lateral meanders in the flow. All five crossings of the A-Front with the MVP showed that the frontal region was well defined by clear gradients in surface temperature and density, though it was best delineated by a sharp subsurface salinity minimum centered at 55 m depth (Fig. 3). This salinity minimum was a prominent feature of the waters to the south of the front (Figs 3 and 4), indicative of waters of higher latitude origins flowing

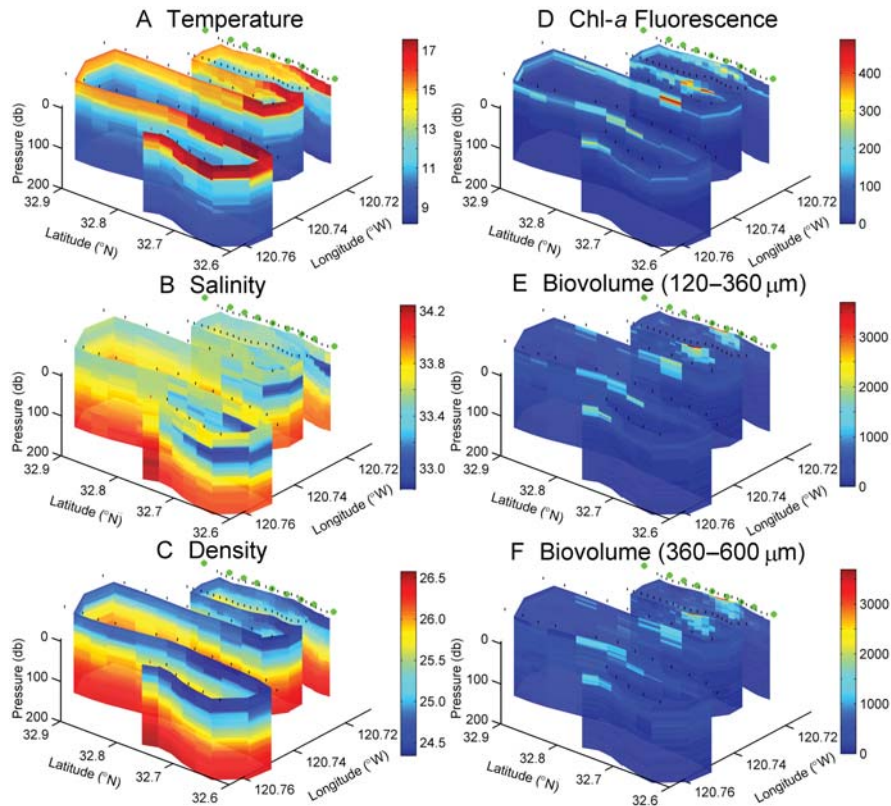


Fig. 3. MVP curtain plots of (A) temperature ($^{\circ}\text{C}$), (B) salinity (psu), (C) density (σ_{θ}), (D) Chl *a* fluorescence (digital counts), (E) particle biovolume 120–360 μm ESD ($\text{mm}^3 \text{m}^{-3}$) and (F) particle biovolume 360–600 μm ESD ($\text{mm}^3 \text{m}^{-3}$). Black ticks indicate locations of MVP casts. Green circles show locations of CTD–UVP5–Rosette casts and bongo samples.

from the north in the core flow of the California Current and then flowing eastward in the vicinity of the A-Front. Salinity, temperature and density sections completed toward the end of the site survey, when horizontal spacing between MVP profiles was shorter, show evidence of subduction of waters from the cooler, northern side of the front toward the south (Fig. 3). Subsurface Chl *a* fluorescence centered on 35 m depth was markedly enhanced in the vicinity of the front, relative to the region both to the north and to the south (Figs 3 and 4). The biovolume of suspended particulate matter was enhanced at the front in all size fractions from 0.1 to 5 mm (Fig. 4). In contrast to Chl *a* fluorescence, which showed subsurface maxima at ~ 35 m depth at the front, the vertical maximum in particle biovolume was near the sea surface (Figs 3 and 4).

The numerical density of all MEP's measured by the LOPC on the MVP was also elevated 4-fold at the front (Fig. 4). Elevated MEP abundances were found throughout the upper 60 m. Figure 5 illustrates coarse-resolution silhouettes of a subset of the MEP's that had an overall opacity of >0.6 and occluded at least four photodiode elements (minimum particle

width ~ 2.5 – 3 mm). North of the A-Front, most of these MEP's are concentrated in the upper 60–90 m of the water column and bear elongate shapes and large body sizes (Fig. 5). Few objects with these shapes were found at the front or south of it. The results in Fig. 5 differ from those in Fig. 4C, in that the latter includes particles with low opacity. The difference between these figures suggests that most of the enrichment of MEP particles at the front (Fig. 4) was due to low-opacity particles, probably indicative of marine snow. The size distribution of MEP's differed substantially across the front, with considerably larger particles found to the north than within or to the south of the front. The normalized particle volume distributions (nVd) reflect this spatial change, with a pronounced peak in biovolume at 4–5 mm that was of much smaller magnitude within or south of the A-Front (Fig. 6). The nVd showed peak biovolume in much smaller size categories at the front (Fig. 6B) again likely attributable to marine snow. No attempt was made to fit slopes to these nVd spectra because of the clear departures from linearity. Examination of the number spectra underlying these volume spectra showed that they were much better

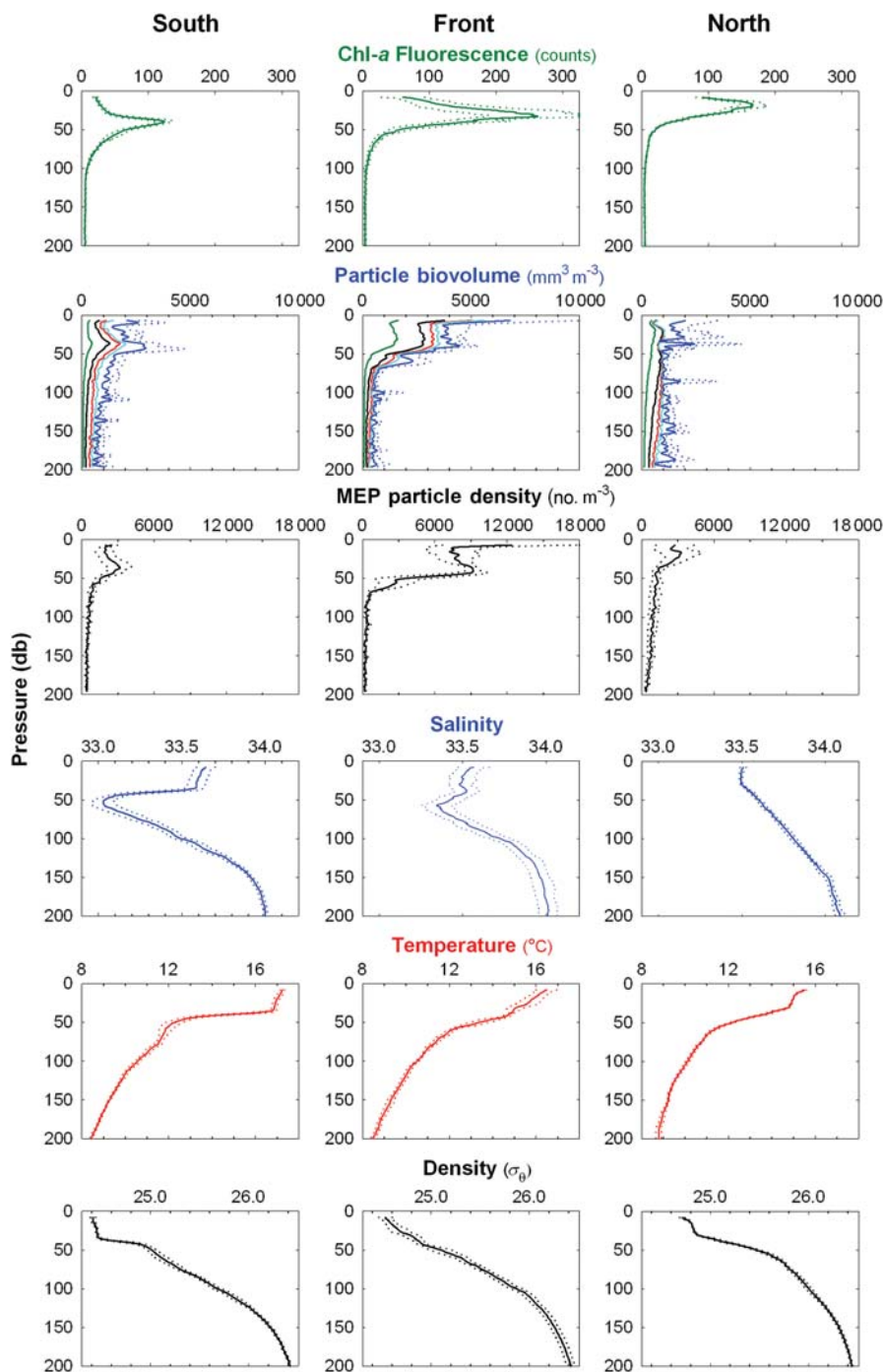


Fig. 4. Mean Moving Vessel vertical profiles at stations South ($n = 11-15$), within ($n = 8-11$) and North ($n = 12-16$) of the A-Front, respectively (solid lines = mean; dotted lines = $\pm 95\%$ CL). Chl *a* fluorescence (digital counts); particle biovolume ($\text{mm}^3 \text{m}^{-3}$) shown in five size categories: green = $120-400 \mu\text{m}$, black $< 800 \mu\text{m}$, red $< 1200 \mu\text{m}$, cyan $< 1600 \mu\text{m}$, blue $< 5000 \mu\text{m}$ ESD; dotted line = upper 95% CL; salinity (psu); temperature ($^{\circ}\text{C}$); density (σ_{θ}).

described by non-linear than linear slopes (data not shown). The mean particle biovolume (in parts per million, ppm), integrated in the upper 200 m from these spectra, was elevated to the north of the

($n\text{Vd} = 2529 \pm 1994 \text{ ppm}$, mean $\pm 95\%$) relative to the front itself ($n\text{Vd} = 1586 \pm 468 \text{ ppm}$) or south of it ($n\text{Vd} = 1966 \pm 508 \text{ ppm}$), although these differences were not statistically significant ($P > 0.05$).

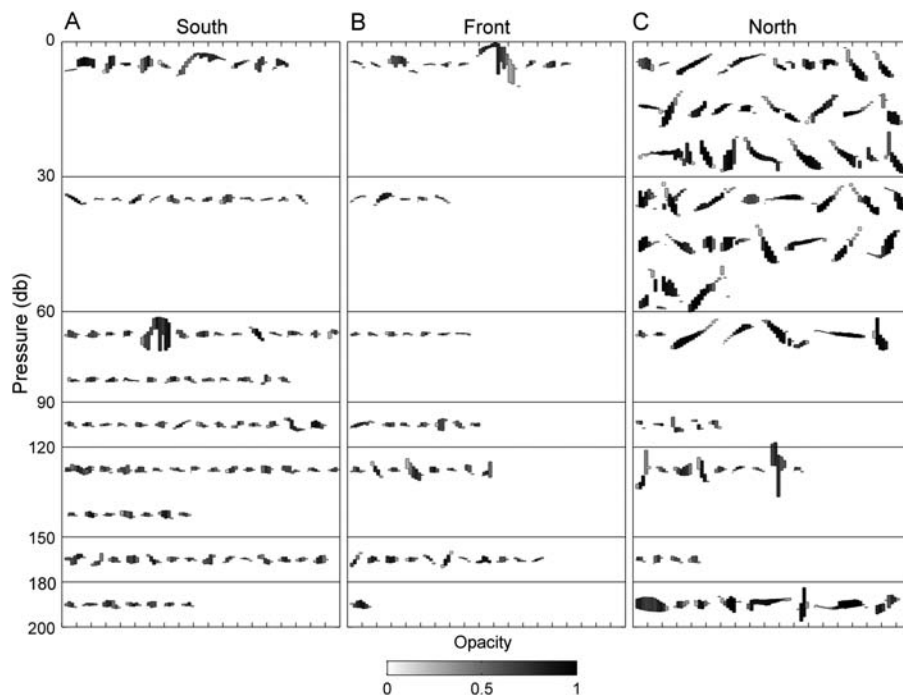


Fig. 5. Vertical profiles illustrating silhouettes of MEP's detected by the MVP-LOPC, for all MEP's ≥ 4 pixels wide and opacity ≥ 0.6 . MEP's are binned in 30 m depth bins for stations (A) south, (B) within and (C) north of the A-Front. The number of objects in each bin is proportional to their relative abundance. Pixels comprising silhouettes are shaded according to the opacity of that pixel; tic marks on the x -axis are separated by 5 mm.

The abundance of several zooplankton taxa enumerated from the vertical bongo tow series changed markedly at the front or nearby. The total net-collected ($>202 \mu\text{m}$) assemblage showed a maximum at the front (Fig. 7, photograph), although this qualitative comparison of plankton samples also includes larger phytoplankton and marine snow particles. Total enumerated mesozooplankton also showed a maximum value at the front. The abundance of calanoid copepods, the cyclopoid copepod *Oithona* spp., euphausiids and euphausiid eggs, as well as the ratio of nauplii total copepods $^{-1}$ showed maxima at the front (Fig. 7). Appendicularia were most abundant within one sampling station (2.8 km) of the peak frontal gradient (Fig. 7). Dividing the sampled stations into those south of the A-Front (stations 1–4) and those in and to the north (stations 5–9), poecilostomatoid copepods, ostracods, chaetognaths and radiolarians were all more abundant to the south of the A-Front (Fig. 7, $P \leq 0.05$, Mann–Whitney U), while *Oithona* spp. and euphausiids were more abundant in the front and to the north ($P \leq 0.05$).

Vertical distributions of selected taxa were characterized across the front from the UVP5 profiles. Many additional types of organisms and particles were recognized in UVP5 images, although they occurred too rarely to resolve vertical distributions accurately. In

accord with the bongo samples taken to 100 m, the radiolarians imaged *in situ* to a depth of 300 m with the UVP5 were considerably more abundant to the south of the front (Fig. 8A). The UVP5 profiles revealed the vertical distribution of the radiolarian assemblage did not change appreciably across the entire frontal cross-section, with distributions extending from 50 to 300 m depth but maxima in abundance concentrated near 100–140 m depth. The abundance of elongate filaments (mean 2.82 mm long \times 0.84 mm wide), some of which resembled fecal pellets, was elevated to the north of the A-Front (Fig. 8B). Organic aggregates, which were defined as more irregularly shaped than the filaments, showed peak abundances at 30–50 m depth at the front (Fig. 8C), with progressively lower abundances and deeper distributions north of the front.

DISCUSSION

We rejected the hypothesis of no difference in mesozooplankton composition and particulate matter occurrence at the frontal discontinuity. The A-Front represented a region transitional between different types of dominant mesozooplankton as well as a site of locally elevated abundance and, apparently, production of some taxa as

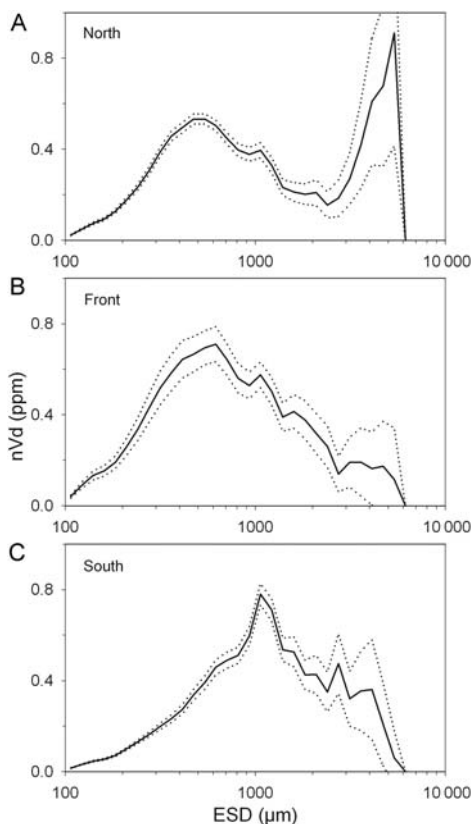


Fig. 6. Normalized volume spectra (nVd, ppm) as a function of particle ESD, for particles detected by the MVP-LOPC for stations (A) north, (B) within and (C) south of the A-Front. Mean (solid line) \pm 95% (dotted lines).

discussed further below. In addition, the A-Front was a region of elevated marine snow particles, as inferred from both the UVP5 and the laser optical plankton counter (LOPC). Other studies conducted in parallel with the present work illustrate a variety of complementary responses from other components of the food web, including elevated bacterial growth rates (Samo *et al.*, 2012), increased photosynthetic quantum yield (H. Wang, personal communication), altered phytoplankton composition (Chekalyuk *et al.*, 2012; Taylor *et al.*, 2012), and altered distributions of some euphausiid species and mesopelagic fishes (Lara-Lopez *et al.*, 2012), suggesting that this feature played a significant role in structuring the plankton assemblage and altering the composition of particulate matter.

We found the free-fall MVP to be an excellent means of characterizing the location and structure of the A-Front, especially since some of the sharpest lateral gradients appeared below the sea surface (e.g. salinity, Chl *a* fluorescence). The MVP profiles only in the vertical plane on descent and, unlike “tow-yo” devices that are towed horizontally while also profiling vertically, the

MVP does not confound vertical with horizontal structures in the water column. Real-time display of MVP data made it possible to respond adaptively at sea to changes in features detected and to direct subsequent sampling efforts. In addition to real-time recognition of the subsurface structure of the front, post-cruise analysis of the repeated MVP-CTD vertical profiles proved useful for characterizing spatial gradients in turbulent energy dissipation (Li *et al.*, 2012). Continuous near-surface horizontal measurements of phytoplankton pigments, CDOM (Chromophoric Dissolved Organic Matter) and variable fluorescence recorded by the Advanced Laser Fluorescence Analyzer (ALF; Chekalyuk *et al.*, 2012) were an excellent complement to the MVP measurements.

We detected pronounced compositional differences of the mesozooplankton at the A-Front. Some taxa, notably calanoid copepods, *Oithona*, euphausiids and appendicularians showed local maxima at the peak frontal gradient region, or adjacent to it. In contrast, other taxa including poecilostomatoid copepods, ostracods, chaetognaths and radiolarians were more abundant in waters south of the front and noticeably less abundant in waters to the north. Although the bongo samples could not be replicated at each station because of time constraints to complete all sampling within nighttime hours, the observed changes occurred relatively smoothly in space, they coincided with other well-defined physical and biotic changes in the water column (see above) and were corroborated by repeated frontal crossings with the MVP.

An advantage of the ZooScan approach to scanning and classification of the preserved zooplankton is relatively rapid scanning and machine classification of digital images, and the ability to simultaneously make accurate size measurements of all objects (Gorsky *et al.*, 2010). Moreover, the images are stored and available for future study, including application of additional classification algorithms as these develop further. Although the subsequent manual validation of images takes additional time, this validation step provides much greater confidence in the resulting taxonomic assignments and size distributional data. A drawback to this digital scanning approach is that it is rarely possible to accurately identify species; hence, the data are expressed at higher taxonomic levels where the identifications can be made correctly. It is likely that there are species-level differences in responses to the front [e.g. within the calanoid copepod category, the euphausiids (see Lara-Lopez *et al.*, 2012) and other taxa], which are not resolved here.

Particularly interesting is the elevated ratio of nauplii copepod⁻¹ at the A-Front, because this suggests locally elevated egg production rates and/or survivorship of

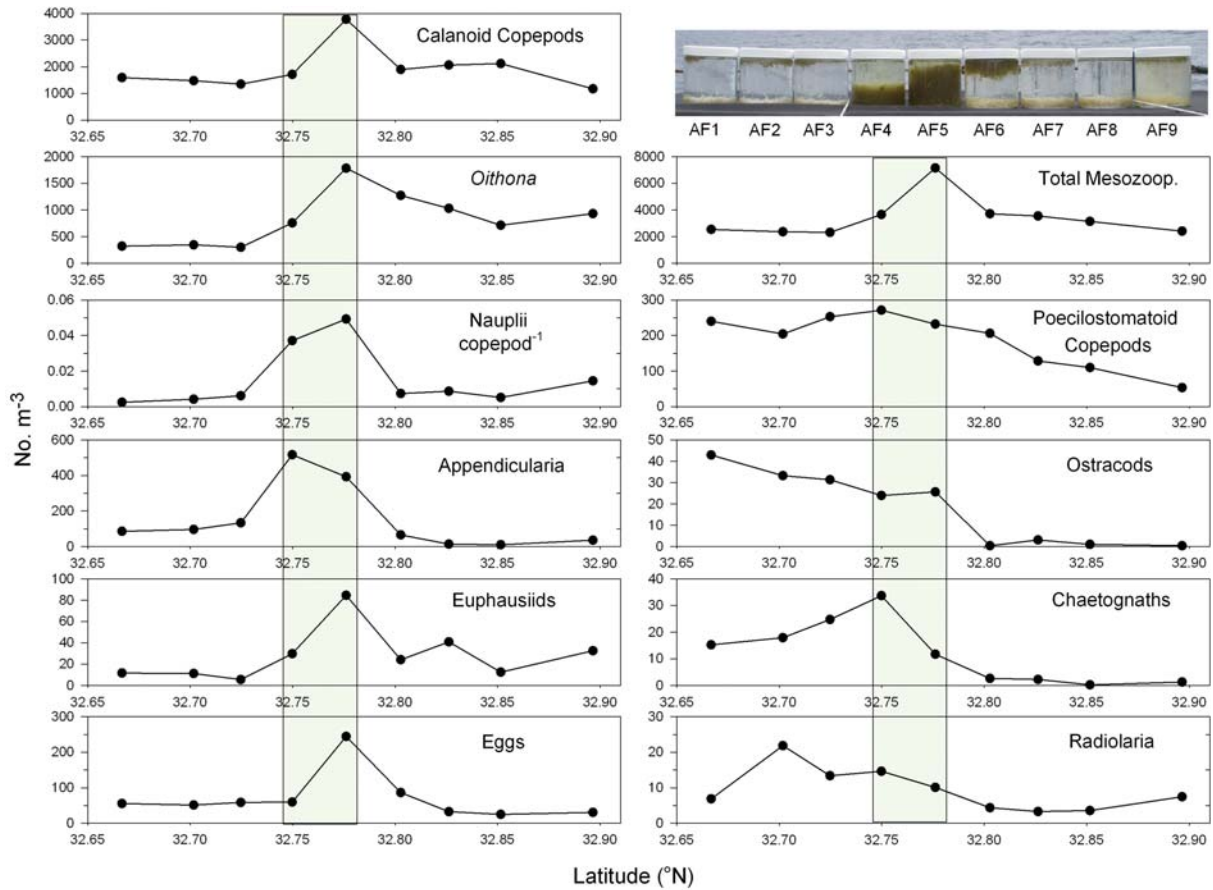


Fig. 7. Vertically integrated abundance ($\text{no.}\cdot\text{m}^{-3}$) of mesozooplankton taxa sampled across the A-Front, from vertical bongo tows analyzed by ZooScan. Photograph in the upper right shows the samples from each of the bongo tows taken across the A-Front. Vertical band illustrates the peak frontal gradient region.

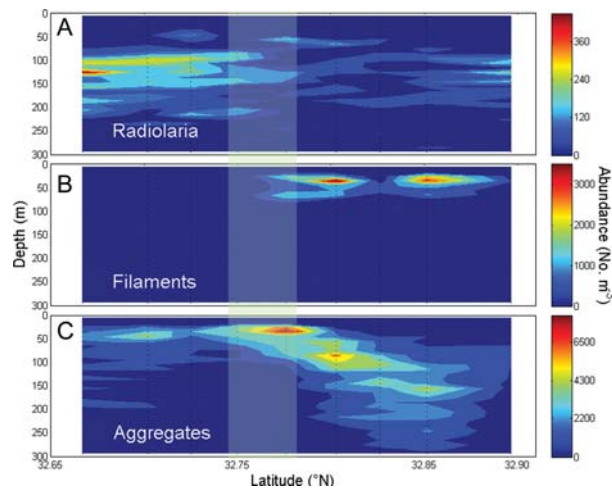


Fig. 8. Vertical profiles of abundance ($\text{no.}\cdot\text{m}^{-3}$) of (A) radiolaria, (B) filaments and (C) organic aggregates sampled across the A-Front by the UVP5. Vertical band illustrates the peak frontal gradient region. Black dots indicate mid-points of the sampled depths, averaged in 10-m depth bins.

eggs and early nauplii. The numerical values of the ratio nauplii copepod⁻¹ are quite low, which is to be expected because of escapement of most nauplii through the 202- μm mesh net and because total copepods are used in the denominator (nauplii could not be differentiated taxonomically into orders from these optical images). Although we would anticipate differential responses among species of calanoids, cyclopoids and poecilostomatoid copepods, nevertheless the overall conclusion is that copepod recruitment was elevated at the frontal location. This suggests that the A-Front was a site of enhanced secondary production, as well as abundance, of several mesozooplankton taxa.

The responses of different mesozooplankton taxa to the A-Front appear to vary with the feeding mode and diet of the organisms considered. The taxa that showed elevated abundances at or near the A-Front were all dominated by particle-grazing zooplankton. Although euphausiids are omnivorous and diets vary by species (Mauchline, 1980; Ohman, 1984), most of the dominant species in this general study area (Lara-Lopez *et al.*, 2012) utilize phytoplankton and microzooplankton prey. Calanoid copepods certainly show diverse feeding modes and the cyclopoid *Oithona* appears to be an ambush grazer that specializes on motile prey (e.g. Paffenhöfer and Mazzocchi, 2002). Nevertheless, most of these copepods, euphausiids and appendicularians primarily utilize suspended microplankton prey, such as the diatoms that were also found to be elevated in the frontal region (Taylor *et al.*, 2012).

In contrast, the mesozooplankton that were elevated to the south of the A-Front were principally carnivorous or marine snow-associated taxa. Chaetognaths are obligate carnivores (Feigenbaum and Maris, 1984). Most of the planktonic ostracods appear to be predatory or scavengers, or omnivorous microphages (Vannier *et al.*, 1998). Radiolarians are diffusion-feeders that are omnivorous; they can ingest smaller zooplankton (Anderson, 1983). And many of the poecilostomatoid copepods are thought to live on or in association with marine snow particles, or to attach to larger prey (Landry *et al.*, 1985). While more needs to be known about the diets and life histories of poecilostomatoids, they can be numerically dominant, especially in more oligotrophic ocean provinces (Böttger-Schnack, 1994), which would agree with their distribution to the south of the front detected here. Hence, we suggest that not only the taxonomic composition, but also the functional characteristics of the mesozooplankton assemblage changed in association with the gradients in production and abundance at the A-Front.

The Underwater Video Profiler provided the added advantage of direct *in situ* imaging of organisms and

detailed localization of their vertical distributions. The radiolarians were present in subsurface waters across our study site, with peak abundances in strata between 100 and 140 m depth. Although radiolaria are certainly known from this region (Isaacs *et al.*, 1971), we were not aware of their nearly ubiquitous distribution and numerical importance in waters below the mixed layer. Their contribution to particle fluxes and silica cycling is an area that merits further attention.

The qualitative silhouettes of larger MEPs as sampled by the LOPC were an immediate indication to us while at sea of spatial changes in the qualitative composition of particulate matter distributed across the A-Front study. Although identification of silhouettes is ambiguous, partly because organisms of uniform size and shape can pass through the LOPC sampling tunnel at different orientations and therefore produce a distribution of different silhouette profiles, even the qualitative information on changes in composition can be useful for guiding subsequent sampling.

The elevated concentrations of organic aggregates and total particle biovolume at or near the site of the peak frontal gradient suggest that this is a site of particle generation and/or aggregation. These results are consistent with the high concentration of diatoms at the front (Chekalyuk *et al.*, 2012; Taylor *et al.*, 2012), which would likely be associated with elevated mesozooplankton grazing and particle production (Dilling *et al.*, 1998), and with the highly elevated rates of bacterial production measured at the front (Samo *et al.*, 2012). Because our surveys were conducted relatively rapidly, we were not able to assess vertical and lateral export fluxes in the vicinity of the A-Front, but we would anticipate enhanced particle export as well as production in this region. Both vertical (cf. Stukel *et al.*, 2012) and lateral (cf. Barth *et al.*, 2002) export fluxes associated with fronts warrant attention in the future.

The A-Front represents an abrupt transition between more offshore and more coastally influenced waters. The offshore (south) side of the front bears a distinctive subsurface salinity minimum, a signature of the California Current proper and an indication of the influence of West Wind Drift-Subarctic waters advected from the north (Lynn and Simpson, 1987). These waters on the offshore side of the front also reflect a history of previous phytoplankton growth, as surface nutrients were depleted to deeper depths than the inshore side (Li *et al.*, 2012). Inshore (to the north) of the front, the somewhat saltier and cooler waters probably originated in the upwelling region off Point Conception (Landry, Ohman, *et al.*, 2012). Another frontal system designated the Ensenada Front has been identified previously in this general region, arising

where the flow of the California Current bifurcates, with some of the water extending eastward into the Southern California Bight and forming the Southern California Eddy, and some of the flow continuing southward along the Baja California coast (e.g. Niiler *et al.*, 1989; Chereskin and Niiler, 1994). The gradient that we have analyzed bears superficial similarities in hydrographic structure to the Ensenada Front, including the warmer surface waters and pronounced subsurface salinity minimum on the offshore side, with somewhat cooler surface waters on the inshore side of the front. However, we saw no evidence of flow bifurcation of the A-Front. Also, previous studies of the Ensenada Front found that “neither shipboard surveys nor remote images suggest enhanced production or accumulation of biomass” at the front (Venrick, 2000). Those results are in marked contrast to the present results from the A-Front study. Although there were differences in the biomass of phytoplankton and mesozooplankton (Haury *et al.*, 1993) and in abundance and taxonomic composition of ichthyoplankton (Moser and Smith, 1993) on opposite sides of the Ensenada Front, that front was not a site of altered plankton concentrations. Our technologies permitted us to sample at approximately an order of magnitude greater spatial resolution than in work done previously at the Ensenada Front, though it seems unlikely that sampling resolution alone accounts for differences in responses that we measured. Because of the differences in ecological consequences and perhaps in secondary circulation, we do not assume that the A-Front is equivalent to the Ensenada Front (see also Landry, Ohman *et al.*, 2012).

Satellite imagery has revealed that ocean fronts are ubiquitous in the world ocean and occur on different spatial scales (Belkin *et al.*, 2009). However, the ecological consequences of such features depend markedly on the specific processes leading to frontogenesis (Franks, 1992) and the time scale of their persistence. As noted in the Introduction section, our deep-water frontal system is not related to topographic features such as the continental shelf break, to tidally related mixing or to riverine buoyancy plumes, all of which can have significant effects on nutrient fluxes and organism growth and aggregation (Holligan, 1981). Nor is the A-Front directly related to nearshore upwelling or associated filaments as often found in eastern boundary current systems (e.g. Hood *et al.*, 1991), hence comparison with such studies must be done cautiously. In addition to their effects on planktonic organisms, some frontal features are well known to be exploited by a variety of higher consumers, including seabirds (Hunt *et al.*, 2002) and fishes

(Lara-Lopez *et al.*, 2012). Ainley *et al.* (Ainley *et al.*, 2009) suggested that seabirds’ spatial distributions in the northern California Current are related to mesoscale physical phenomena, including fronts, when their prey are abundant, but are more closely related to smaller scale prey patches when prey are rare, implying flexible responses.

The question remains whether the elevated abundances of some taxa are best accounted for by local, *in situ* production because of enhanced prey availability at the A-Front or by physical aggregation associated with secondary circulation features (cf. Cromwell and Reid, 1956; Franks, 1992). The elevated phytoplankton photosynthetic quantum yield (H. Wang, personal communication), inferred increases in vertical fluxes of nutrients in the region at or just south of the A-Front (Li *et al.*, 2012) and the presence of highly elevated diatom biomass at the front (Taylor *et al.*, 2012) show that this was a region of locally elevated primary production. This region also corresponded to enhanced nauplii per copepod, suggesting enhanced secondary production. However, some of the mesozooplankton taxa that showed elevated abundances at the A-Front, such as copepods and euphausiids, have generation times that can extend to weeks or even months, which establishes the necessary persistence time scale of the front if *in situ* population growth alone were to account for the observed elevated abundances. It seems likely that some aspects of local, convergent flow also contribute to enhanced abundances in this region (cf., Chereskin and Niiler, 1994). Directed studies are needed to resolve the secondary vertical and horizontal flows associated with such frontal features, and their consequences for organisms with different degrees of motility (Franks, 1992).

In summary, the A-Front represented a significant gradient in mesozooplankton composition, with a tendency toward more carnivorous taxa on the southern side of the front and more herbivorous/omnivorous taxa at or on the northern side of the front. In the narrow frontal region itself, a number of particle-feeding taxa showed elevated abundances that are consistent with the elevated concentrations of larger phytoplankton, especially diatoms. The frontal region was also a site of elevated concentrations of suspended particle matter, especially in the form of diffuse marine snow particles, presumably originating from enhanced particulate production, grazing and aggregation. Long-term changes in the occurrence of such features (e.g. Kahru *et al.*, 2012) can have significant consequences for the biogeochemistry of pelagic ecosystems.

ACKNOWLEDGEMENTS

We thank all participants in the CCE-LTER process cruises, and D.M. Checkley and M.R. Landry for comments on the manuscript.

FUNDING

This work was supported by the U.S. National Science Foundation via the California Current Ecosystem Long-Term Ecological Research site; and by the Gordon and Betty Moore Foundation.

REFERENCES

- Ainley, D. G., Dugger, K. D., Ford, R. G. *et al.* (2009) Association of predators and prey at frontal features in the California Current: competition, facilitation, and co-occurrence. *Mar. Ecol. Progr. Ser.*, **389**, 271–294.
- Anderson, O. R. (1983) *Radiolaria*. Springer, New York.
- Barth, J. A., Cowles, T. J., Kosro, P. M. *et al.* (2002) Injection of carbon from the shelf to offshore beneath the euphotic zone in the California Current. *J. Geophys. Res.*, **107**, 3057.
- Barth, J. A., Pierce, S. D. and Cowles, T. J. (2005) Mesoscale structure and its seasonal evolution in the northern California Current System. *Deep-Sea Res. II*, **52**, 5–28.
- Belkin, I. M., Cornillon, P. C. and Sherman, K. (2009) Fronts in large marine ecosystems. *Progr. Oceanogr.*, **81**, 223–236.
- BOT (2005). *Laser Optical Plankton Counter Operation and Maintenance Manual*. Brooke Ocean Technology Ltd, OM-0400-0-04-01A. pp. 1–37.
- Böttger-Schnack, R. (1994) The microcopepod fauna in the Eastern Mediterranean and Arabian seas: a comparison with the Red Sea fauna. *Hydrobiologia*, **292/293**, 271–282.
- Brinton, E., Ohman, M. D., Townsend, A. W. *et al.* (1999) *Euphausiids of the World Ocean*. Vol. CD-ROM, MacIntosh version 1.0, UNESCO Publishing, Paris.
- Checkley, D. M. Jr., Davis, R. E., Herman, A. W. *et al.* (2008) Assessing plankton and other particles in situ with the SOLOPC. *Limnol. Oceanogr.*, **53**, 2123–2136.
- Chekalyuk, A., Landry, M. R., Goericke, R. *et al.* (2012) Laser fluorescence analysis of phytoplankton across a frontal zone in the California Current ecosystem. *J. Plankton Res.*, **34**, 761–777.
- Chereskin, T. K. and Niiler, P. P. (1994) Circulation in the Ensenada Front—September 1988. *Deep-Sea Res.*, **41**, 1251–1287.
- Cowles, T. J., Desiderio, R. A. and Carr, M. E. (1998) Small-scale planktonic structure: persistence and trophic consequences. *Oceanography*, **11**, 4–9.
- Cromwell, T. and Reid, J. L. (1956) A study of oceanic fronts. *Tellus*, **8**, 94–101.
- Davis, R. E., Ohman, M. D., Rudnick, D. L. *et al.* (2008) Glider surveillance of physics and biology in the southern California Current System. *Limnol. Oceanogr.*, **53**, 2151–2168.
- Dilling, L., Wilson, J., Steinberg, D. *et al.* (1998) Feeding by the euphausiid *Euphausia pacifica* and the copepod *Calanus pacificus* on marine snow. *Mar. Ecol. Progr. Ser.*, **170**, 189–201.
- Feigenbaum, D. L. and Maris, R. C. (1984) Feeding in the Chaetognatha. *Oceanogr. Mar. Biol. Annu. Rev.*, **22**, 343–392.
- Franks, P. J. S. (1992) Sink or swim—accumulation of biomass at fronts. *Mar. Ecol. Progr. Ser.*, **82**, 1–12.
- Gaardsted, E., Tande, K. S. and Basedow, S. L. (2010) Measuring copepod abundance in deep-water winter habitats in the NE Norwegian Sea: intercomparison of results from laser optical plankton counter and multinet. *Fish. Oceanogr.*, **19**, 480–492.
- Genin, A., Greene, C., Haury, L. *et al.* (1994) Zooplankton patch dynamics: daily gap formation over abrupt topography. *Deep-Sea Res.*, **41**, 941–951.
- Gorsky, G., Ohman, M. D., Picheral, M. *et al.* (2010) Digital zooplankton image analysis using the ZooScan integrated system. *J. Plankton Res.*, **32**, 285–303.
- Haury, L. R. (1984) An offshore eddy in the California Current System. Part IV: plankton distributions. *Prog. Oceanogr.*, **13**, 95–111.
- Haury, L. R., McGowan, J. A. and Wiebe, P. H. (1978) Patterns and processes in the time-space scales of plankton distributions. In: Steele, J. H. (ed). *Spatial Pattern in Plankton Communities*, Plenum, New York, pp. 277–327.
- Haury, L. R., Venrick, E. L., Fey, C. L. *et al.* (1993) The Ensenada Front—July 1985. *CalCOFI Reports*, **34**, 69–88.
- Herman, A.W., Beanlands, B., Chin-Yee, M. *et al.* (1998) The Moving Vessel Profiler (MVP): in-situ sampling of plankton and physical parameters at 12 kts and the integration of a new Laser Optical Plankton (LOPC) Counter. <http://www.alexherman.com/pub002.php>
- Herman, A. W., Beanlands, B. and Phillips, E. F. (2004) The next generation of Optical Plankton Counter: the Laser-OPC. *J. Plankton Res.*, **26**, 1135–1145.
- Holligan, P. M. (1981) Biological implications of fronts on the north-west European continental shelf. *Phil. Trans. Roy. Soc. Lond. Ser. Am.*, **302**, 547–562.
- Hood, R. R., Abbott, M. R. and Huyer, A. (1991) Phytoplankton and photosynthetic light response in the Coastal Transition Zone off northern California in June 1987. *J. Geophys. Res.*, **96**, 14769–14780.
- Hunt, G. L., Baduini, C. and Jahncke, J. (2002) Diets of short-tailed shearwaters in the southeastern Bering Sea. *Deep-Sea Res. II*, **49**, 6147–6156.
- Hunt, G. L., Russell, R. W., Coyle, K. O. *et al.* (1998) Comparative foraging ecology of planktivorous auklets in relation to ocean physics and prey availability. *Mar. Ecol. Progr. Ser.*, **167**, 241–259.
- Isaacs, J. D., Fleminger, A. and Miller, J. K. (1971) Distributional atlas of zooplankton biomass in the California Current region: Winter, 1955–1959. *CalCOFI Atlas*, **14**, 1–122.
- Jackson, G. A., Maffione, R., Costello, D. K. *et al.* (1997) Particle size spectra between 1 μm and 1 cm at Monterey Bay determined using multiple instruments. *Deep-Sea Res. I*, **44**, 1739–1767.
- Kahru, M., Di Lorenzo, E., Manzano-Sarabia, M. *et al.* (2012) Spatial and temporal statistics of sea surface temperature and chlorophyll fronts in the California Current. *J. Plankton Res.*, **34**, 749–760.
- Landry, M. R., Lehner-Fournier, J. M. and Fagerness, V. L. (1985) Predatory feeding behavior of the marine cyclopoid copepod *Corycaeus anglicus*. *Mar. Biol.*, **85**, 163–169.

- Landry, M. R., Ohman, M. D., Goericke, R. *et al.* (2012) Pelagic community responses to a deep-water front in the California Current Ecosystem: overview of the A-Front study. *J. Plankton Res.*, **34**, 739–748.
- Lara-Lopez, A. L., Davison, P. and Koslow, J. A. (2012) Abundance and community composition of micronekton across a frontal system off Southern California. *J. Plankton Res.*, **34**, 828–848.
- Li, Q. P., Franks, P. J. S., Ohman, M. D. *et al.* (2012) Enhanced nitrate fluxes and biological processes at a frontal zone in the southern California Current System. *J. Plankton Res.*, **34**, 790–801.
- Lynn, R. J. and Simpson, J. J. (1987) The California Current System: the seasonal variability of its physical characteristics. *J. Geophys. Res.*, **92**, 12947–12966.
- Mackas, D. L., Washburn, L. and Smith, S. L. (1991) Zooplankton community pattern associated with a California Current cold filament. *J. Geophys. Res.*, **96**(C8), 14781–14797.
- Mauchline, J. (1980) The biology of mysids and euphausiids. *Adv. Mar. Biol.*, **18**, 1–677.
- Moser, H. G. and Smith, P. E. (1993) Larval fish assemblages of the California Current region and their horizontal and vertical distributions across a front. *Bull. Mar. Sci.*, **53**, 645–691.
- Nüller, P. P., Poulain, P. M. and Haury, L. R. (1989) Synoptic 3-dimensional circulation in an offshore-flowing filament of the California Current. *Deep-Sea Res.*, **36**, 385–405.
- Ohman, M. D. (1984) Omnivory by *Euphausia pacifica*: the role of copepod prey. *Mar. Ecol. Progr. Ser.*, **19**, 125–131.
- Ohman, M. D. and Wilkinson, J. R. (1989) Comparative standing stocks of mesozooplankton and macrozooplankton in the southern sector of the California Current System. *Fish. Bull.*, **87**, 967–976.
- Owen, R. W. (1991) Microscale and finescale variations of small plankton in coastal and pelagic environments. *J. Mar. Res.*, **47**, 197–240.
- Paffenhöfer, G.-A. and Mazzocchi, M. G. (2002) On some aspects of the behaviour of *Oithona plumifera* (Copepoda: Cyclopoida). *J. Plankton Res.*, **24**, 129–135.
- Peterson, W. T., Miller, C. B. and Hutchinson, A. (1979) Zonation and maintenance of copepod populations in the Oregon upwelling zone. *Deep-Sea Res. II*, **26**, 467–494.
- Picheral, M., Guidi, L., Stemann, L. *et al.* (2010) The Underwater Vision Profiler 5: an advanced instrument for high spatial resolution studies of particle size spectra and zooplankton. *Limnol. Oceanogr. Meth.*, **8**, 462–473.
- Pingree, R. D. and Griffiths, D. K. (1978) Tidal fronts on the shelf seas around the British Isles. *J. Geophys. Res. Oceans Atm.*, **83**, 4615–4622.
- Prairie, J. C., Franks, P. J. S. and Jaffe, J. S. (2010) Cryptic peaks: invisible vertical structure in fluorescent particles revealed using a planar laser imaging fluorometer. *Limnol. Oceanogr.*, **55**, 1943–1958.
- Samo, T. J., Pedler, B. E., Ball, G. I. *et al.* (2012) Microbial distribution and activity across a water mass frontal zone in the California Current Ecosystem. *J. Plankton Res.*, **34**, 802–814.
- Schultes, S. and Lopes, R. M. (2009) Laser Optical Plankton Counter and Zooscan intercomparison in tropical and subtropical marine ecosystems. *Limnol. Oceanogr. Meth.*, **7**, 771–784.
- Smith, S. L. and Lane, P. V. Z. (1991) The jet off Point Arena, California: its role in aspects of secondary production in the copepod *Eucalanus californicus* Johnson. *J. Geophys. Res. Oceans*, **96**, 14849–14858.
- Stukel, M. R., Landry, M. R., Ohman, M. D. *et al.* (2012) Do inverse ecosystem models accurately reconstruct plankton trophic flows? Comparing two solution methods using field data from the California Current. *J. Mar. Syst.*, **91**, 20–33.
- Taylor, A. G., Goericke, R., Landry, M. R. *et al.* (2012) Sharp gradients in phytoplankton community structure across a frontal zone in the California Current Ecosystem. *J. Plankton Res.*, **34**, 778–789.
- Vannier, J., Abe, K. and Ikuta, K. (1998) Feeding in myodocopid ostracods: functional morphology and laboratory observations from videos. *Mar. Biol.*, **132**, 391–408.
- Venrick, E. L. (2000) Summer in the Ensenada Front: the distribution of phytoplankton species, July 1985 and September 1988. *J. Plankton Res.*, **22**, 813–841.